

Nonradial stability of topological stars

Alexandru Dima,^{1,2,*} Marco Melis,^{1,2,†} and Paolo Pani^{1,2,‡}

¹*Dipartimento di Fisica, Sapienza Università di Roma, Piazzale Aldo Moro 5, 00185, Roma, Italy*

²*INFN, Sezione di Roma, Piazzale Aldo Moro 2, 00185, Roma, Italy*

Topological stars are regular, horizonless solitons arising from dimensional compactification of Einstein-Maxwell theory in five dimensions, which could describe qualitative properties of microstate geometries for astrophysical black holes. They also provide a compelling realization of ultracompact objects arising from a well-defined theory and display all the phenomenological features typically associated with black hole mimickers, including a (stable) photon sphere, long-lived quasinormal modes, and echoes in the ringdown. By completing a thorough linear stability analysis, we provide strong numerical evidence that these solutions are stable against nonradial perturbations with zero Kaluza-Klein momentum.

CONTENTS

I. Introduction	1
II. Theoretical framework	2
III. Numerical methods	3
IV. Results	4
V. Conclusions	5
Acknowledgments	6
A. Regge-Wheeler-Zerilli ansatz for 5D linear perturbations	6
B. Evolution equations for linear perturbations	9
1. Type-II, $l \geq 2$	9
2. Type-II, $l = 1$	12
References	14

I. INTRODUCTION

An outstanding challenge related to black holes (BHs) is providing a microscopic interpretation of their entropy, which is famously equal to the horizon area in Planck units [1], and consequently enormous for astrophysical BHs. A compelling explanation for this entropy is given by the fuzzball paradigm of string theory, according to which a classical BH can be interpreted as a thermodynamical approximation of a huge number of regular quantum states [2–4]. In the classical limit, the latter are described by “microstate geometries”: solitons with the same mass and charges as a BH, but with a drastically different inner geometry, wherein the horizon is

replaced by a smooth horizonless cap [5–9]. The absence of an event horizon in the fundamental description automatically resolves Hawking’s information loss paradox [10, 11], since information can be retrieved by the horizon structure provided by the microstate geometries.

Two key ingredients of the fuzzball construction are the intrinsically higher dimensionality of the microstate solutions and their nontrivial topologies, which prevent the horizon-scale structure from collapsing. While the microstates characterizing horizon-scale structure are smooth, topologically nontrivial geometries in ten dimensions, in four dimensions they appear to have curvature singularities [12, 13]. These solutions are particularly involved and, from the four-dimensional perspective, do not have any spatial isometries. This has so far prevented dynamical studies, which would instead be highly informative about the linear stability and out-of-equilibrium dynamics of these solutions (see Ref. [14] for an exception considering a test scalar field).

A particularly simple model incorporating some of the key fuzzball ideas was proposed some years ago in [15], which discovered regular solitons in Einstein-Maxwell theory in five dimensions. These solutions were dubbed topological stars (TSs) since they have topological cycles supported by the magnetic flux. TSs have several appealing features. Their four-dimensional reduction (upon compactifying the fifth dimension on a circle) asymptotically resembles magnetic BHs, but lacks an event horizon, while the 5D counterpart remains free of curvature singularities. They can be macroscopically large compared to the size of the Kaluza-Klein circle so they could describe qualitative properties of microstate geometries for astrophysical BHs. Furthermore, their gravitational potential smoothly interpolates between that of a moderately compact star and that of an ultracompact object which could mimic the peculiar phenomenological features of BHs [16]. Finally, extensions of these solutions can be constructed such that they are globally neutral and asymptote to a Schwarzschild BH [9], although at the expenses of introducing more complexity and breaking spherical symmetry.

The spherical symmetry of the simplest TSs is also particularly convenient to study the properties of these solutions, for example performing ray tracing [17], studying

* alexandru.dima@uniroma1.it

† marco.melis@uniroma1.it

‡ paolo.pani@uniroma1.it

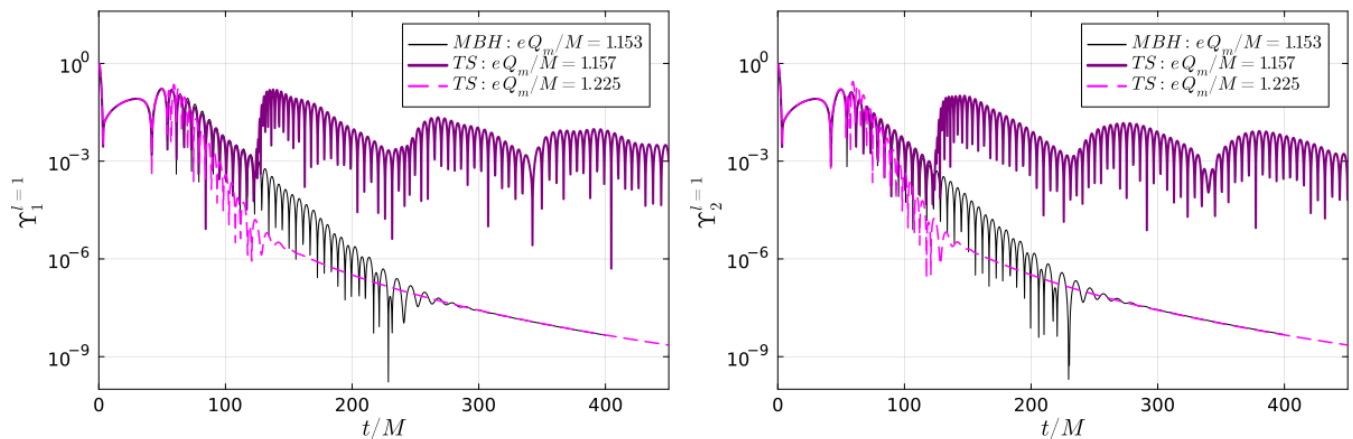


FIG. 1. Comparison between the linear response of a nearly-extremal magnetized BH (black) and a second-kind TS with same mass and similar charge-to-mass ratio (purple) to $l = 1$ Type-II perturbations (odd-parity electromagnetic, and even-parity scalar). The left and right panels refer to scalar-driven and electromagnetic-driven perturbations, respectively. For comparison we show also the case of a first-kind TS (magenta), which displays a different prompt ringdown and no long-lived modes.

the dynamics of test fields [18, 19] and, recently, their linear response [20–23]. In particular, Refs. [20, 21] studied the linear dynamics of TSs, to compute their quasinormal modes (QNMs) and ringdown waveform. The presence of a background magnetic field mixes perturbations with opposite parity, but still allows for separating them in two independent sectors, dubbed Type I and Type II (see below for details). The Type I sector was found to be free of instabilities. The Type II sector is significantly more involved and only radial perturbations (that belong to this sector) were analyzed in [20, 21]. In this case there exists a radial unstable mode with momentum along the fifth direction, which is directly connected to the Gregory-Laflamme instability [24] of charged black strings [25–27]. However, this mode only affects TSs with small compactness, leaving the most interesting region of the parameter space available.

Here we continue the linear stability of TSs by analyzing the nonradial Type II perturbations with zero Kaluza-Klein momentum. As we shall discuss, also in this sector we do not find any signature for instability, suggesting that TSs are stable against nonradial perturbations.

A representative example of our analysis is shown in Fig. 1, which compares the time-domain linear response of a magnetized BH with different families of TSs. As we shall discuss in detail, the ringdown of very compact (second-kind, see classification below) TSs is initially very similar to that of a BH and displays slowly-decaying echoes [20, 28–30] at late time, whereas less compact (first-kind) TSs display a standard exponentially suppressed ringdown, but with different modes compared to the BH case.

II. THEORETICAL FRAMEWORK

We consider Einstein-Maxwell theory in 5D,

$$S_5 = \int d^5x \sqrt{-g} \left(\frac{1}{2\kappa_5^2} \mathbf{R} - \frac{1}{4} \mathbf{F}_{AB} \mathbf{F}^{AB} \right). \quad (1)$$

Differently from what was done in [20], here we do not perform a four-dimensional compactification, and keep working in the 5D picture. Thus, we consider the TS and magnetized BH found in [15] as our background solutions, which are described by the five-dimensional line element¹

$$ds^2 = -f_S dt^2 + f_B dy^2 + \frac{1}{h} dr^2 + r^2 d\Omega_2^2 \quad (2)$$

$$F = P \sin \theta d\theta \wedge d\phi \quad (3)$$

where

$$f_S = 1 - \frac{r_S}{r}, \quad f_B = 1 - \frac{r_B}{r},$$

$$h = f_B f_S, \quad P = \pm \frac{1}{\kappa_5} \sqrt{\frac{3r_S r_B}{2}}. \quad (4)$$

The mass and magnetic charge of the solution are $M = \frac{2\pi}{\kappa_4^2} (2r_S + r_B)$ and $Q_m = \frac{1}{\kappa_4} \sqrt{\frac{3}{2}} r_S r_B$, respectively, where we introduced the effective coupling constant in 4D defined as $\kappa_4^2 := \kappa_5^2 / (2\pi R_y)$, with R_y the radius of the compact extra dimension². The TS solution corresponds

¹ Although we work in 5D, we will always have in mind a Kaluza-Klein compactification of the y dimension on a circle with radius R_y . Having in mind their 4D version, we will refer to these solutions as (magnetized) BHs and TSs, although in 5D they are actually strings.

² See [31] for a discussion about the relative size of r_B and R_y .

to the region $r_B > r_S$, whereas $r_B < r_S$ corresponds to a magnetized BH with event horizon located at $r = r_S$. For a TS, the metric compactified to 4D diverges at $r = r_B$, which corresponds to a curvature singularity, but the solution is perfectly regular in the five dimensional uplift.

We can classify TSs in two families, according to the number of photon spheres in their spacetime [18, 19, 32]: if $3/2 < r_B/r_S \leq 2$, the solution has a single unstable photon sphere at the boundary $r_{\text{ph}}^{(1)} = r_B$ (*first-kind* TS), whereas if $1 \leq r_B/r_S \leq 3/2$ the solution (*second-kind* TS) has a stable photon sphere at $r_{\text{ph}}^{(2)} = r_B$ and an unstable one at $r_{\text{ph}}^{(1)} = \frac{3}{2}r_S$, just like the magnetized BH solution. Thus, second-kind TSs classify as ultracompact objects [16]: their stable photon-sphere can support long-lived QNMs [18–21, 33], and their response in the time domain is initially very similar to that of a BH with comparable charge-to-mass ratio, while their late time response is governed by echoes [18, 20, 28–30], analogously to what observed for test scalar perturbations of microstate geometries [14].

The linear perturbations of TSs have been derived in [20, 21], to which we refer for all details (see also [34, 35]). The so-called Type-I sector contains odd-parity gravitational perturbations coupled to even-parity electromagnetic perturbations, whereas the Type-II sector contains even-parity gravitational and scalar perturbations coupled to odd-parity electromagnetic ones³. Here we focus on Type-II nonradial perturbations, that are more involved and never studied so far.

Due to the spherical symmetry of the background, it is convenient to expand the perturbations in a basis of (scalar, vector, tensor) spherical harmonics of even and odd parity [20] (see Appendix A). Beside the spherical mode ($l = 0$, where l is the harmonic index) studied in [20, 21], the next-to-simplest Type-II mode is the dipole ($l = 1$). In this case, we introduce auxiliary dynamical fields $\{\Upsilon_1, \Upsilon_2\}$, which correspond, respectively, to scalar-driven and electromagnetic-driven perturbations; and, in addition, a constrained perturbation Λ to close the system. One can derive (see Appendix B for the derivation) the evolution equations for the two dynamical degrees of freedom corresponding to Type-II perturbations with $l = 1$:

$$\mathcal{D}[\Upsilon_i] + \sum_{j=1,2} W_{ij} \partial_r \Upsilon_j - \sum_{j=1,2} V_{ij} \Upsilon_j = 0 \quad (5)$$

where $i, j = 1, 2$ and we introduced the differential operator $\mathcal{D} = \omega^2 + (f_B f_S^2) \partial_r^2$. The coefficients appearing in Eq. (5) are reported in extended form in Appendix B.

For $l \geq 2$, there are three dynamical degrees of freedom: a scalar, an odd-parity electromagnetic, and an

even-parity gravitational mode. They are described by the equations:

$$\begin{aligned} \mathcal{D}[\tilde{\Upsilon}_i] + \sum_{j=1,2,3} \tilde{W}_{ij} \partial_r \tilde{\Upsilon}_j - \sum_{j=1,2,3} \tilde{V}_{ij} \tilde{\Upsilon}_j \\ + \sum_{j=1,2,3} \tilde{U}_{ij} \partial_r^2 \tilde{\Upsilon}_j = 0 \end{aligned} \quad (6)$$

where $\{\tilde{\Upsilon}\}_{i=1,2,3} = \{\Phi, \mathcal{B}, \mathcal{R}^+\}$ are the scalar-driven, electromagnetic-driven and gravity-driven perturbation fields. Once again, we refer to Appendix B for the details about the definition of the variables, $\tilde{\Upsilon}_i$, the explicit expression of the coefficients, $\{\tilde{U}_{ij}, \tilde{W}_{ij}, \tilde{V}_{ij}\}$, and the derivation of Eqs. (6).

III. NUMERICAL METHODS

We solve the sets of equations (5) and (6) respectively for $l = 1$ and $l = 2$ Type-II perturbations both in the frequency domain, as an eigenvalue problem to compute the QNMs, and in the time domain, as an initial value problem to study the linear response of the solution.

We use the same boundary conditions and numerical techniques discussed in [20], to which we refer for more details. In particular, both sets of equations (5) and (6) are Heun equations which possess a regular singular point at $r = r_B$. A Fuchsian analysis of the solutions expanded around the singular point allows us to identify the appropriate boundary conditions that are needed to ensure that linear perturbations on a TS background are regular [20].

In contrast to [20], where the perturbations equations were decoupled and of the Schrödinger-like form, in this case Eqs. (5) and (6) are coupled, both for $l = 1$ and $l \geq 2$. In this regard, for the computation of the QNMs we use a matrix-valued direct integration method as discussed in detail in [37, 38]. For an array of perturbations $\{\Upsilon\}_{j=1,2}$ (similarly for $\{\tilde{\Upsilon}\}_{j=1,2,3}$) we consider the following series expansions near r_B (the same holds for the magnetized BH case, near r_S)

$$\Upsilon^{(j)} = (r - r_B)^\lambda \sum_{i=0}^{\infty} c_i^{(j)} (r - r_B)^i, \quad (7)$$

where λ is fixed by the Fuchsian analysis, and we choose an orthogonal basis of unit vectors for the N -dimensional space, $c_0^{(1)} = (1, 0, 0, \dots, 0)$, $c_0^{(2)} = (0, 1, 0, \dots, 0)$, ..., $c_0^{(N)} = (0, 0, 0, \dots, 1)$. At infinity the solution is given by a linear combination of ingoing and outgoing waves

$$\Upsilon^{(j)} \sim B^{(j)} e^{-i\omega r} r^{\tilde{\lambda}} + C^{(j)} e^{i\omega r} r^{-\tilde{\lambda}}, \quad (8)$$

where again $\tilde{\lambda}$ is fixed by the Fuchsian analysis. To compute the QNMs we request only outgoing waves to survive. For the present case of a system of N coupled

³ Alternatively, one could use an electromagnetic duality transformation to avoid coupling perturbations with opposite parity [21, 36].

second order ODEs we use the orthogonal basis of the N -dimensional space and after performing N integrations from the inner boundary to infinity we construct the following $N \times N$ matrix

$$\mathbf{S}(\omega) = \begin{pmatrix} B_1^{(1)} & B_1^{(2)} & \dots & B_1^{(N)} \\ B_2^{(1)} & B_2^{(2)} & \dots & \dots \\ \dots & \dots & \dots & \dots \\ \dots & \dots & \dots & \dots \\ B_N^{(1)} & \dots & \dots & B_N^{(N)} \end{pmatrix} \quad (9)$$

and we impose $\det \mathbf{S}(\omega) = 0$, which is the condition defining the QNMs.

For the time-domain computations, we follow the same approach as [20]. The evolution equations are integrated using the method of lines. Spatial derivatives are discretized with a fourth-order finite-difference stencil, and time stepping is performed using a fourth-order Runge-Kutta method. At the outer boundary of the computational grid we impose outgoing radiative boundary conditions with a fourth-order finite difference approximation, which help reduce the numerical noise from the boundary. At the inner boundary, we carefully implemented boundary conditions to ensure regularity or radiative behavior depending on the nature of the object (namely TS or BH). We also incorporate techniques to improve numerical stability and accuracy, such as adaptive stretching of the computational domain and long simulations to capture long-lived modes [20]. After obtaining the time-domain signal, QNMs are extracted by performing a Fourier transform and fitting the peaks in the frequency spectrum (see Fig. 2 for an example). This approach ensures consistency between frequency-domain and time-domain computations, enabling detailed analysis of the linear response and stability of the studied systems.

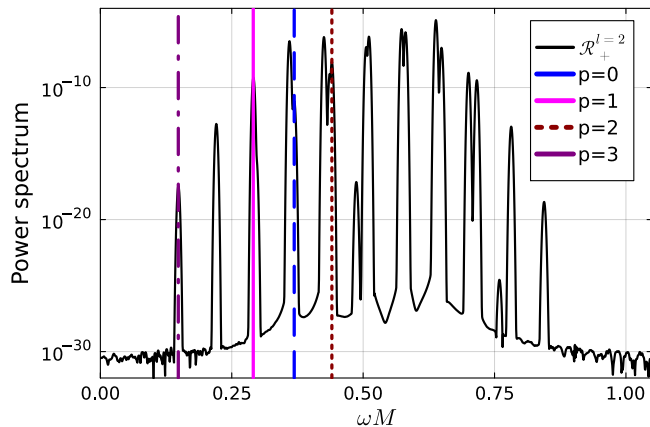


FIG. 2. Power spectrum of Type-II perturbations with $l = 2$ around a second-kind TS with $r_S/r_B = 0.99$, showing the peaks corresponding to the long-lived modes reported in Table II, which are labeled by an integer $p = 0, 1, 2, 3$. The remaining modes are stable and sub-dominant (i.e. more damped) with respect to the labeled ones.

IV. RESULTS

In this section we present the linear-perturbation analysis of magnetized BHs and TSs, both in the frequency- and in the time-domain. We order the QNMs accordingly to their imaginary part and label them with an integer $p = 0, 1, 2, \dots$, with $p = 0$ denoting the mode with the smallest imaginary part (in absolute value). Note that this classification does not differentiate among modes belonging to different families (i.e., gravitational-, electromagnetic-, or scalar-driven).

The results for magnetized BHs are summarized in Fig. 3 for $l = 1$ (top panels) and $l = 2$ (bottom panels). For $l = 2$, we have 3 different families of modes associated to the gravitational-, electromagnetic-, and scalar-driven perturbations in the neutral limit ($Q_m \rightarrow 0$) which are all coupled to each other for nonvanishing Q_m . For $l = 1$, we have the same effect both for electromagnetic- and scalar-driven modes only, since the gravitational ones do not propagate. The markers shown in the plots corresponds to the modes extracted from the Fourier transform of the time-domain signal (see Fig. 2 for an example of the power spectrum in the TS case, and Ref. [20] for technical details).

The agreement between the frequency- and the time-domain methods is overall very good, especially for the frequency of the mode. This is quantified in Table I for few selected cases and the first three tones.

Let us now summarize the results for the Type-II QNMs of TSs. We show the most relevant modes for $l = 1, 2$ in Fig. 4. In this case we show different modes ($p = 0, 1, 2$), since they would be relevant to accurately fit the time-domain response, as we shall later discuss. Note that the mode hierarchy depends on the charge, since there are crossings in the imaginary part. We classify $p = 0, 1, 2, \dots$ modes referring to the region near the BH transition (i.e., smallest value of eQ_m/M). Also in this case we present a comparison between the QNMs computed in the frequency domain and those extracted from the time response (see Table II), showing very good agreement.

As already noted for the Type-I sector [20], the QNM spectrum of a TS smoothly interpolates from BH-like modes for first-kind TSs, to long-lived modes as the TS becomes of the second kind.

Because of these long-lived modes, it is natural to ask whether there exist nonradial unstable modes (which, within our conventions, are defined by a QNM with positive imaginary part). We have scanned the parameter space of TSs searching for such unstable modes and did not found any. This is also confirmed by the time domain response, which is always decaying in time. Some representative examples are shown in Fig. 5 for the scalar-driven, electromagnetic-driven, and gravitational-driven modes of a magnetized BH, second-kind TSs with similar charge-to-mass ratio, and a first-kind TS. As discussed in Ref. [20] for Type-I perturbations, also in this case we observe that the ringdown of a second-kind TS

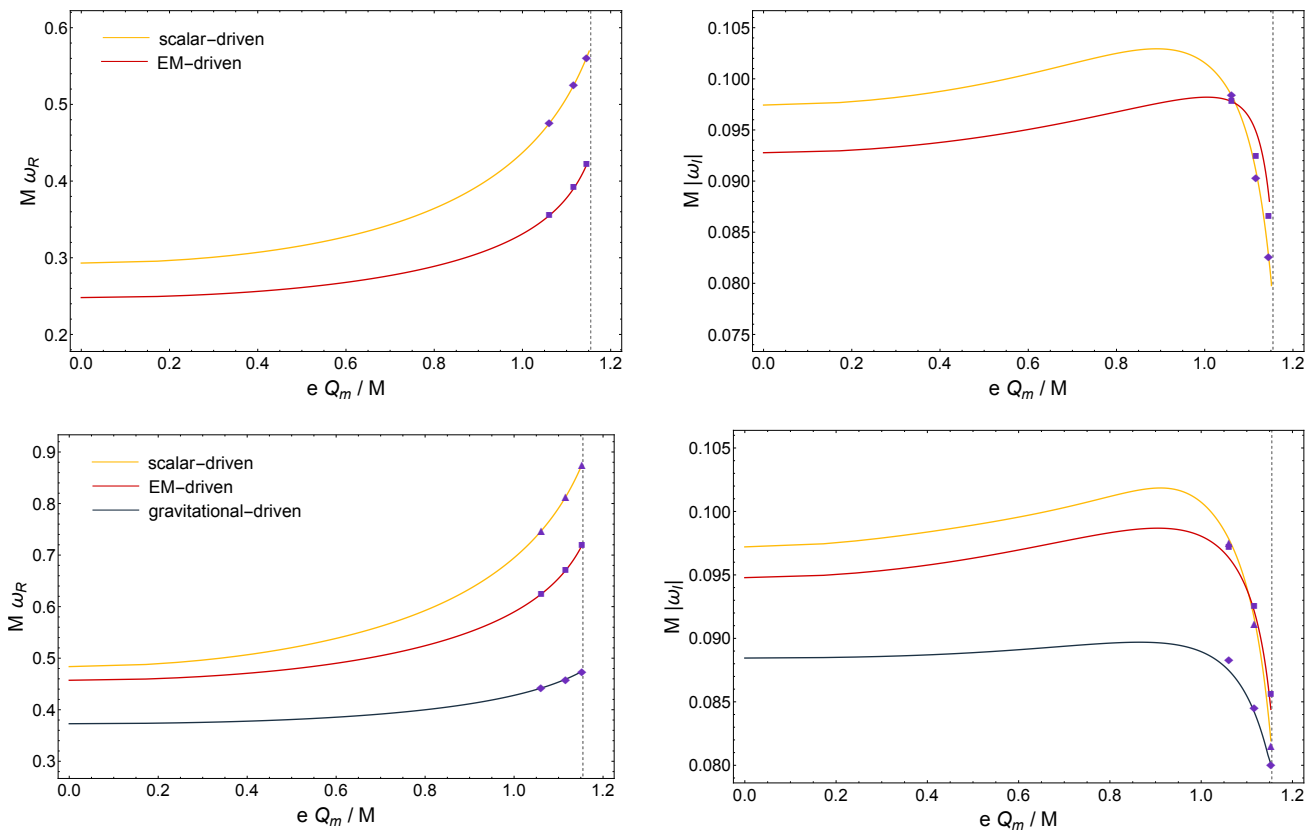


FIG. 3. QNMs of a magnetized BH as a function of the magnetic charge for Type-II perturbations. Top panels refer to $l = 1$, electromagnetic and scalar perturbations, while bottom panels refer to $l = 2$ gravitational, electromagnetic, and scalar perturbations. The left (right) panels show the real (imaginary) part of the mode. In the limit $r_B \rightarrow 0$, i.e. $Q_m \rightarrow 0$, the frequencies are those of the fundamental QNMs for test scalar, vector and spin-2 tensor fields in the background of the Schwarzschild BH. The vertical dashed line denotes the extremal BH. The solid lines were obtained with the f-domain method, while the markers correspond to the modes extracted from the Fourier transform of the time-domain signal. We classify the modes based on the hierarchy also in terms of p : for $l = 1$, $p = 0, 1$ correspond to electromagnetic- and scalar-driven modes, respectively; whereas for $l = 2$, $p = 0, 1, 2$ correspond to gravitational-, electromagnetic- and scalar-driven modes, respectively.

can be initially very similar to that of a BH with similar charge-to-mass ratio, whereas differences appear at late times in the form of (slowly decaying) echoes arising from the absence of a horizon in the TS spacetime. On the other hand, less compact (first-kind) TSs display a standard exponentially suppressed ringdown, but with different modes compared to the BH case.

Finally, we also note that TSs have the same late-time, power-law tail as BHs [39], regardless of the charge-to-mass ratio. While the scaling in time of the tail is due to low-frequency backscattering off the potential and is indeed universal and independent of the nature of the object, it is interesting to note that the amplitude of the tails seems also universal. We have checked that the latter depends only on the amplitude of the initial data and not on the underlying solutions.

V. CONCLUSIONS

We studied nonradial perturbations of magnetized BHs and TSs with zero momentum along the fifth dimension, providing strong numerical evidence for the linear stability of these solutions in a region not affected by the known Gregory-Laflamme-like instability for radial perturbations. It would be interesting to explore if the stability results extend also for nonradial perturbations with nonzero Kaluza-Klein momentum. This would require a generalization of the perturbation ansatz, since more perturbations of the five-dimensional fields would be allowed in the presence of Kaluza-Klein momentum.

A natural follow-up consists in verifying the stability under nonlinear perturbations, especially for TSs of the second kind, which feature a stable photon sphere. Indeed, there are arguments suggesting that ultracompact objects might be unstable at the nonlinear level [33, 40]. This is due to the slow (possibly logarithmic) decay in time of their characteristic modes, as discussed for mi-

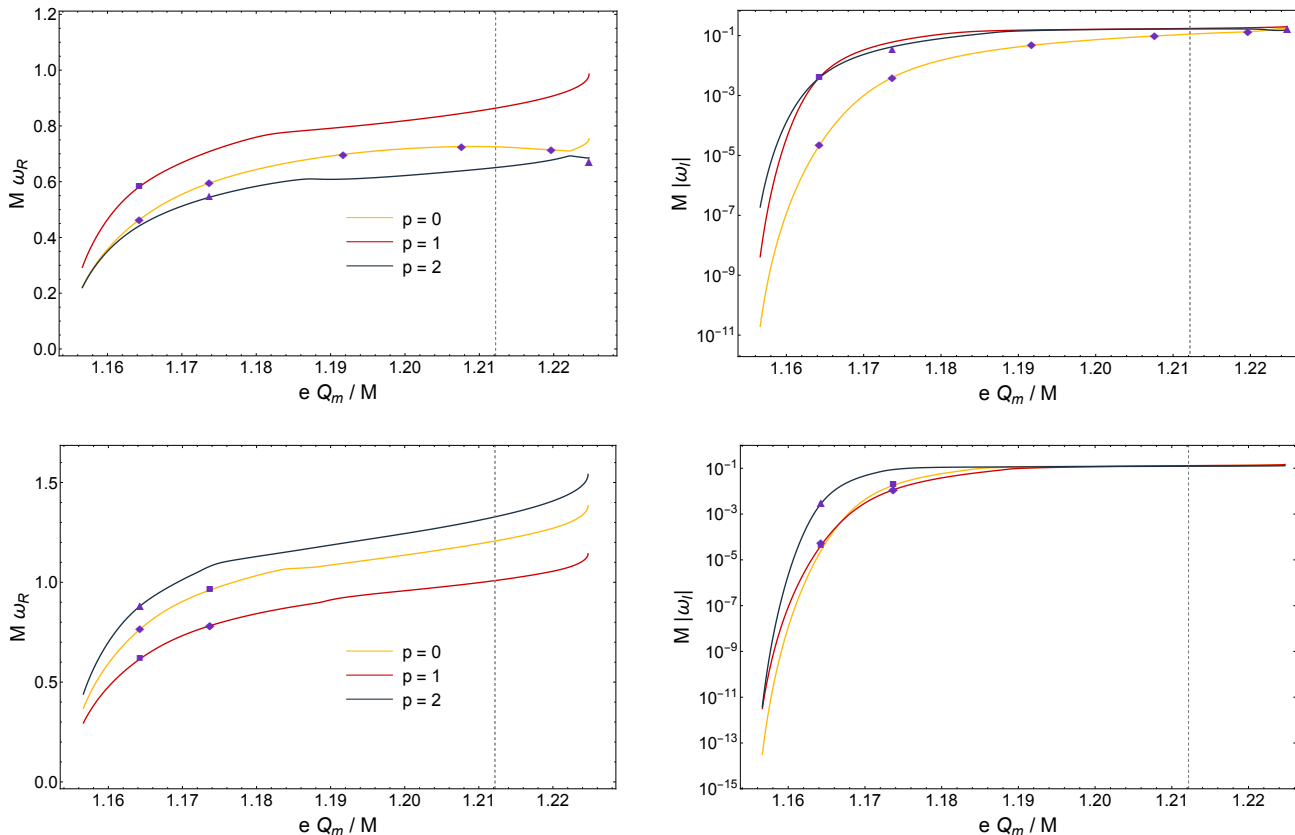


FIG. 4. The first $p = 0, 1, 2$ QNMs of a TS as a function of the magnetic charge for Type-II, $l = 1$ (top panels) and $l = 2$ (bottom panels) perturbations. The left (right) panels show the real (imaginary) part of the mode. The vertical dashed line denotes the transition between second-kind and first-kind TS. The markers corresponds to the modes extracted from the Fourier transform of the time-domain signal. Note that the mode hierarchy (labeled by p) depends on the charge, since there are crossings in the imaginary part.

crostate geometries [41] and for other ultracompact objects [33, 42]. TSs provide a well-defined model in which the nonlinear evolution of the perturbations can be possibly studied in a relatively simple setting.

Finally, our results can be also useful to study the gravitational-wave emission from a point particle orbiting a TS, as recently studied for a test scalar field [23].

ACKNOWLEDGMENTS

We are indebted to Nicola Franchini for enlightening discussions, comments on the draft, and for spotting an error in the initial approach to the special case $l = 1$. This work is partially supported by the MUR PRIN

Grant 2020KR4KN2 “String Theory as a bridge between Gauge Theories and Quantum Gravity”, by the FARE programme (GW-NEXT, CUP: B84I20000100001), and by the INFN TEONGRAV initiative. Some numerical computations have been performed at the Vera cluster supported by the Italian Ministry for Research and by Sapienza University of Rome.

Appendix A: Regge-Wheeler-Zerilli ansatz for 5D linear perturbations

We employ an extended Regge-Wheeler ansatz for 5D perturbations (see [36] for a discussion on how to fix the gauge starting from the most general ansatz), to decouple the angular dependence:

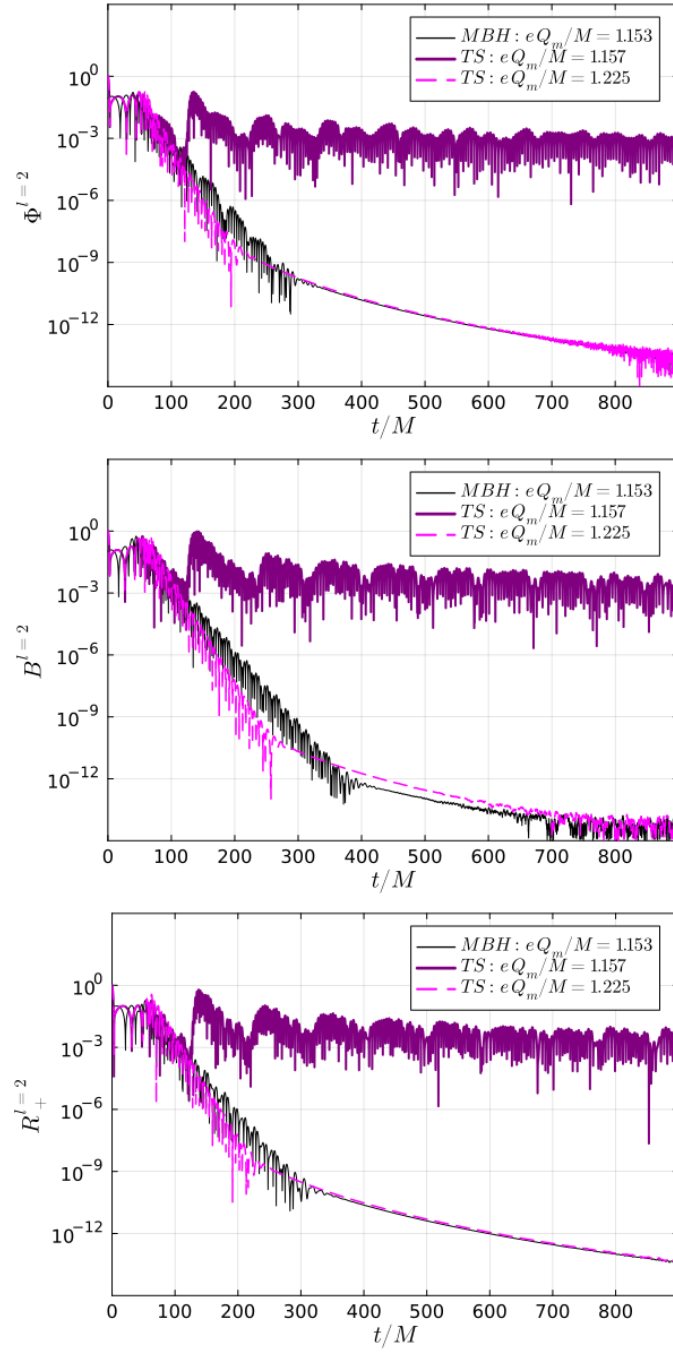


FIG. 5. Comparison between the linear response of a nearly-extremal magnetized BH (black), a second-kind TS with same mass and similar charge-to-mass ratio (purple), and a first-kind TS (magenta) to $l = 2$ even-parity (Type-II) perturbations. Top, middle, and bottom panels refer to scalar-driven, electromagnetic-driven, and gravitational-driven perturbations, respectively.

$r_S/r_B =$			3/2	6/5	105/100	101/100
$l = 1$	$p = 0$	f-domain	$0.475099 - i 9.839 \times 10^{-2}$	$0.524964 - i 9.099 \times 10^{-2}$	$0.560557 - i 8.253 \times 10^{-2}$	$0.571244 - i 7.323 \times 10^{-2}$
		t-domain	$0.475190 - i 9.838 \times 10^{-2}$	$0.525453 - i 9.027 \times 10^{-2}$	$0.560590 - i 8.253 \times 10^{-2}$	$0.571628 - i 7.295 \times 10^{-2}$
	$p = 1$	f-domain	$0.354988 - i 9.783 \times 10^{-2}$	$0.390223 - i 9.481 \times 10^{-2}$	$0.420558 - i 8.874 \times 10^{-2}$	$0.435112 - i 8.038 \times 10^{-2}$
		t-domain	$0.354371 - i 9.776 \times 10^{-2}$	$0.390621 - i 9.238 \times 10^{-2}$	$0.421263 - i 8.647 \times 10^{-2}$	$0.436811 - i 7.940 \times 10^{-2}$
$r_S/r_B =$			3/2	6/5	105/100	101/100
$l = 2$	$p = 0$	f-domain	$0.746666 - i 9.787 \times 10^{-2}$	$0.813286 - i 9.169 \times 10^{-2}$	$0.860856 - i 8.465 \times 10^{-2}$	$0.875909 - i 8.194 \times 10^{-2}$
		t-domain	$0.746698 - i 9.754 \times 10^{-2}$	$0.812986 - i 9.114 \times 10^{-2}$	$0.860790 - i 8.451 \times 10^{-2}$	$0.875271 - i 8.151 \times 10^{-2}$
	$p = 1$	f-domain	$0.623768 - i 9.629 \times 10^{-2}$	$0.670552 - i 9.213 \times 10^{-2}$	$0.706721 - i 8.691 \times 10^{-2}$	$0.719101 - i 8.441 \times 10^{-2}$
		t-domain	$0.622475 - i 9.716 \times 10^{-2}$	$0.670021 - i 9.250 \times 10^{-2}$	$0.706936 - i 8.659 \times 10^{-2}$	$0.717444 - i 8.551 \times 10^{-2}$
	$p = 2$	f-domain	$0.441539 - i 8.722 \times 10^{-2}$	$0.458477 - i 8.424 \times 10^{-2}$	$0.470346 - i 8.122 \times 10^{-2}$	$0.473974 - i 8.009 \times 10^{-2}$
		t-domain	$0.441655 - i 8.832 \times 10^{-2}$	$0.458697 - i 8.449 \times 10^{-2}$	$0.470706 - i 8.112 \times 10^{-2}$	$0.473640 - i 8.005 \times 10^{-2}$

TABLE I. Type-II QNMs of magnetized BH with $eQ_m/M \approx \{1.061, 1.116, 1.153\}$ for $l = 1$ (top table) and $l = 2$ (bottom table). Modes with $p = 0, 1$ correspond to scalar-driven and electromagnetic-driven perturbations, whereas $p = 2$ denotes gravitational-driven perturbations (which are not dynamical for $l = 1$).

$r_S/r_B =$			7/10	9/10	19/20	99/100	
$l = 1$	$p = 0$	f-domain	$0.725735 - i 9.739 \times 10^{-2}$	$0.594653 - i 3.979 \times 10^{-3}$	$0.463193 - i 2.163 \times 10^{-5}$	$0.221521 - i 1.967 \times 10^{-11}$	
		t-domain	$0.725753 - i 9.735 \times 10^{-2}$	$0.594636 - i 3.978 \times 10^{-3}$	$0.463183 - i 2.160 \times 10^{-5}$	$0.221438 - i 2.110 \times 10^{-11}$	
	$p = 1$	f-domain	-	$0.543775 - i 4.233 \times 10^{-2}$	$0.581303 - i 4.013 \times 10^{-3}$	$0.293106 - i 4.147 \times 10^{-9}$	
		t-domain	-	$0.549296 - i 3.719 \times 10^{-2}$	$0.581265 - i 4.006 \times 10^{-3}$	$0.292507 - i 4.089 \times 10^{-9}$	
	$p = 2$	f-domain	-	$0.708010 - i 6.095 \times 10^{-2}$	$0.441270 - i 3.926 \times 10^{-3}$	$0.220050 - i 1.896 \times 10^{-7}$	
		t-domain	-	$0.709243 - i 5.997 \times 10^{-2}$	$0.441245 - i 3.910 \times 10^{-3}$	$0.220049 - i 1.875 \times 10^{-7}$	
	$p = 3$	f-domain	-	-	$0.681979 - i 3.779 \times 10^{-2}$	$0.362912 - i 2.424 \times 10^{-7}$	
		t-domain	-	-	$0.682161 - i 3.173 \times 10^{-2}$	$0.362168 - i 2.329 \times 10^{-7}$	
	$r_S/r_B =$			7/10	9/10	19/20	99/100
	$l = 2$	$p = 0$	f-domain	$0.569028 - i 4.955 \times 10^{-2}$	$0.834579 - i 1.619 \times 10^{-4}$	$0.630961 - i 2.895 \times 10^{-8}$	$0.368629 - i 3.221 \times 10^{-14}$
t-domain			$0.569024 - i 4.981 \times 10^{-2}$	$0.834486 - i 1.865 \times 10^{-4}$	$0.630844 - i 3.245 \times 10^{-8}$	$0.368733 - i (*)$	
$p = 1$		f-domain	$1.085261 - i 7.599 \times 10^{-2}$	$0.422771 - i 6.856 \times 10^{-4}$	$0.317783 - i 5.510 \times 10^{-6}$	$0.295274 - i 3.206 \times 10^{-12}$	
		t-domain	$1.085059 - i 7.557 \times 10^{-2}$	$0.424131 - i 7.271 \times 10^{-4}$	$0.317827 - i 5.551 \times 10^{-6}$	$0.295660 - i (*)$	
$p = 2$		f-domain	-	$0.782183 - i 1.144 \times 10^{-2}$	$0.764893 - i 2.534 \times 10^{-5}$	$0.439992 - i 3.944 \times 10^{-12}$	
		t-domain	-	$0.782285 - i 1.146 \times 10^{-2}$	$0.765489 - i 3.821 \times 10^{-5}$	$0.440391 - i (*)$	
$p = 3$		f-domain	-	$0.960878 - i 1.792 \times 10^{-2}$	$0.616095 - i 4.239 \times 10^{-5}$	$0.148446 - i 6.337 \times 10^{-11}$	
		t-domain	-	$0.961672 - i 1.825 \times 10^{-2}$	$0.616099 - i 4.103 \times 10^{-5}$	$0.148477 - i 6.262 \times 10^{-11}$	

TABLE II. Same as in Table I but for TSs with $eQ_m/M \approx \{1.208, 1.174, 1.164, 1.157\}$ (equivalently, $r_S/r_B = \{0.70, 0.90, 0.95, 0.99\}$). The asterisk indicates QNMs with a characteristic damping time that is too large for the spectral analysis to retrieve an accurate fit thereof.

$$h_{AB}^{\text{even}} = \sum_{l,m} \begin{pmatrix} f_S H_0(t, y, r) & H_4(t, y, r) & H_1(t, y, r) & 0 & 0 \\ * & f_B H_3(t, y, r) & H_5(t, y, r) & 0 & 0 \\ * & * & (f_S f_B)^{-1} H_2(t, y, r) & 0 & 0 \\ 0 & 0 & 0 & r^2 K(t, y, r) & 0 \\ 0 & 0 & 0 & 0 & r^2 \sin^2 \theta K(t, y, r) \end{pmatrix} Y_{lm}(\theta, \phi), \quad (\text{A1})$$

$$h_{AB}^{\text{odd}} = \sum_{l,m} \begin{pmatrix} 0 & 0 & 0 & -h_0(t, y, r)/\sin \theta \partial_\phi & h_0(t, y, r) \sin \theta \partial_\theta \\ 0 & 0 & 0 & -h_2(t, y, r)/\sin \theta \partial_\phi & h_2(t, y, r) \sin \theta \partial_\theta \\ 0 & 0 & 0 & -h_1(t, y, r)/\sin \theta \partial_\phi & h_1(t, y, r) \sin \theta \partial_\theta \\ * & * & * & 0 & 0 \\ * & * & * & 0 & 0 \end{pmatrix} Y_{lm}(\theta, \phi), \quad (\text{A2})$$

$$f_{AB}^{\text{even}} = \sum_{l,m} \begin{pmatrix} 0 & f_{ty}^+(t, y, r) & f_{tr}^+(t, y, r) & f_{t\theta}^+(t, y, r) \partial_\theta & f_{t\phi}^+(t, y, r) \partial_\phi \\ \cdot & 0 & f_{yr}^+(t, y, r) & f_{y\theta}^+(t, y, r) \partial_\theta & f_{y\phi}^+(t, y, r) \partial_\phi \\ \cdot & \cdot & 0 & f_{r\theta}^+(t, y, r) \partial_\theta & f_{r\phi}^+(t, y, r) \partial_\phi \\ \cdot & \cdot & \cdot & 0 & 0 \\ \cdot & \cdot & \cdot & 0 & 0 \end{pmatrix} Y_{lm}(\theta, \phi), \quad (\text{A3})$$

$$f_{AB}^{\text{odd}} = \sum_{l,m} \begin{pmatrix} 0 & 0 & 0 & f_{t\theta}^-(t, y, r)/\sin \theta \partial_\phi & -f_{t\theta}^-(t, y, r) \sin \theta \partial_\theta \\ 0 & 0 & 0 & f_{y\theta}^-(t, y, r)/\sin \theta \partial_\phi & -f_{y\theta}^-(t, y, r) \sin \theta \partial_\theta \\ 0 & 0 & 0 & f_{r\theta}^-(t, y, r)/\sin \theta \partial_\phi & -f_{r\theta}^-(t, y, r) \sin \theta \partial_\theta \\ \cdot & \cdot & \cdot & 0 & l(l+1) f_{\theta\phi}^-(t, y, r) \sin \theta \\ \cdot & \cdot & \cdot & \cdot & 0 \end{pmatrix} Y_{lm}(\theta, \phi). \quad (\text{A4})$$

where the uppercase Latin indices span the coordinates $A, B = \{t, y, r, \theta, \phi\}$. The asterisks, *, (respectively, dots, \cdot) indicate symmetry (respectively, antisymmetry) with respect to the corresponding upper-half matrix elements.

Furthermore, because the background possesses two isometries in the t and y directions, we can further decouple the time and fifth-dimension dependence by:

$$A(t, y, r) = e^{-i\omega t} e^{i\sigma y} a(r) \quad (\text{A5})$$

where A is the generic perturbation field. In this work, we restrict to consider the scenario in which the fifth dimension is compactified, our compact objects are macroscopic and effectively 4D and, thus, excitations in the fifth dimension are negligible, $\sigma = 0$ (see the discussion in [20]).

Appendix B: Evolution equations for linear perturbations

By applying the ansätze (A1) and (A5) to the field equations, and keeping only linear terms, one obtains a set of first- and second-order partial differential equations that can be further recast to obtain the evolution equations for the proper independent dynamical degrees of freedom. Because of the magnetic charge of the background, the perturbations will be coupled together in the

equations according to two groups: Type-I perturbations (h_{AB}^{odd} and f_{AB}^{even}) and Type-II perturbations (h_{AB}^{even} and f_{AB}^{odd}). The first group (as well as the special case $l = 0$ from the second) have been studied and discussed in [20]. Here, we shall focus on the solution and discussion of Type-II perturbations in the two cases, $l = 1$ and $l \geq 2$.

1. Type-II, $l \geq 2$

The derivation of the system of equations (6) valid for the generic case $l \geq 2$ involves some cumbersome manipulations, thus here we will summarize the main idea and discuss only the key steps.

First, we proceed by taking the limit $\sigma \rightarrow 0$, which is the most interesting one for macroscopic objects. Then, we can eliminate H_2 from all equations by employing the (θ) component of the Einstein equations. Next, by combining the (t) , (r) and (ϕ) components, an equation can be obtained that relates H_0 to an algebraic combination of H_1 , K , $f_{\theta\phi}^-$, H_3 and first derivatives thereof. This relation can be inverted to eliminate H_0 from the system of equations just as we did for H_2 .

With the elimination of H_0 , H_2 , we can construct a second-order equation for H_3 via a linear combination of (y) , (θ) components of the linearized Einstein equations, in addition to the second-order equation for $f_{\theta\phi}^-$, which is provided by the θ -component of the linearized Maxwell

equation. In addition, the linearized Einstein equations are reduced to a system of two first-order equations for H_1 and K . We then proceed to generalize Zerilli's procedure to reduce the system of two first-order equations to a single second-order equation for an auxiliary variable that encodes the gravitational degree of freedom. To do so, we introduce two auxiliary variables $\hat{\Psi} = (\hat{K}, \hat{H})$ linked to $\Psi = (K, H_1)$ via $\Psi = \mathbf{F}\hat{\Psi}$, and such that the original system of first-order equations

$$\frac{d\Psi}{dr} = \mathbf{A} \cdot \Psi + \mathcal{S} \quad (\text{B1})$$

reduces to

$$\frac{d\hat{\Psi}}{dr_*} = \mathbf{B} \cdot \hat{\Psi} + \hat{\mathcal{S}}, \quad (\text{B2})$$

where we introduced the generic coordinate $dr_* = n(r)^{-1}dr$. The matrix elements of \mathbf{A} are known, the elements of \mathbf{F} are unknown and we fix the form of \mathbf{B} to be

$$\mathbf{B} = \begin{pmatrix} q(r) & 1 \\ V_0(r) - \omega^2 & p(r) \end{pmatrix} \quad (\text{B3})$$

where $p(r)$, $q(r)$ and $V_0(r)$ are also free to be fixed.

One can notice that the equations above imply the following system:

$$n(r)\mathbf{F}^{-1} \left((\mathbf{A}\mathbf{F} - \frac{d\mathbf{F}}{dr}) \right) - \mathbf{B} = 0 \quad (\text{B4})$$

which can be solved to fix \mathbf{F} and \mathbf{B} . This step is as crucial as delicate. We first fix $n(r) := (\sqrt{f_B}f_S)^{-1}$, in such a way that the coordinate r_* is the appropriate tortoise one for our background ⁴.

The result of this procedure can be summed up in the relations:

$$\begin{aligned} K &= -\frac{(1+3f_B)}{8rf_B\zeta_B} \partial_r \hat{K} - \frac{3+4\lambda+3f_B(f_S-1)-3f_S}{8r^2f_Bf_S\zeta_B} \hat{K} \\ &\quad - \frac{P\kappa_5^2(1+3f_B)^2f_S}{4r^2f_B\zeta_B} f_{\theta\phi}^- + \frac{r(1+3f_B)f_S}{4\zeta_B} \partial_r H_3 \\ &\quad + \frac{(1+3f_B)(2f_S+f_B(3f_S-1))}{8f_B\zeta_B} H_3 \end{aligned} \quad (\text{B5})$$

$$H_1 = -\frac{4r}{f_S(1+3f_B)} K - \frac{1}{rf_Bf_S^2(1+3f_B)} \hat{K} \quad (\text{B6})$$

where $2\lambda = (l-1)(l+2)$ and $8f_B\zeta_B = f_B^2(6-15f_S) + 2f_B(9+8\lambda-6f_S) + 3f_S$. As final steps, we introduce $\mathcal{R}^+ := \hat{K} - 2r^2f_Bf_SH_3$, $\Phi := H_3/f_B$ and $\mathcal{B} := f_{\theta\phi}^-/\kappa_5$, to help us simplify the equations and obtain the final system (6) with coefficients defined as:

⁴ For more details on the tortoise coordinate and its adaptation to

both magnetized BH and TS backgrounds, see discussion in [20].

$$\tilde{U}_{ij} = -\delta_{i1}\delta_{j3} \frac{(1-f_B)^2 f_S^3}{4\zeta_B} \quad (\text{B7})$$

$$\tilde{W}_{11} = -\frac{f_S}{8r\zeta_B} \left((15+16\lambda-9f_S)f_S - 2f_B(9+8\lambda+(9+16\lambda)f_S) + 3f_B^2(-2+f_S+11f_S^2) \right) \quad (\text{B8})$$

$$\tilde{W}_{12} = -\frac{P\kappa_5(1-f_B)f_S^2}{4r^3\zeta_B} \left(-2f_B(9+8\lambda-8f_S) - f_S + f_B^2(-6+9f_S) \right) \quad (\text{B9})$$

$$\begin{aligned} \tilde{W}_{13} = & -\frac{(1-f_B)f_B f_S^2}{64r f_B^2 \zeta_B^2} \left(f_S(-33-32\lambda+39f_S) + f_B(6(9+8\lambda) + (111+112\lambda)f_S - 87f_S^2) \right. \\ & \left. + f_B^2(108+80\lambda - (267+208\lambda)f_S - 15f_S^2) + 15f_B^3(2-13f_S+17f_S^2) \right) \end{aligned} \quad (\text{B10})$$

$$\begin{aligned} \tilde{V}_{11} = & \frac{f_S}{64r^2 f_B^2 \zeta_B^2} \left(9(7+6\lambda-3f_S)f_S^2 + f_B f_S(189+312\lambda+128\lambda^2 - 15(21+16\lambda)f_S + 72f_S^2) \right. \\ & - 3f_B^4(66+72\lambda-6(31+28\lambda)f_S + 7(27+2\lambda)f_S^2 - 201f_S^3) + 2f_B^2((7+4\lambda)(9+8\lambda)^2 - (927+1404\lambda+512\lambda^2)f_S \\ & + 6(96+71\lambda)f_S^2 - 72f_S^3) + 9f_B^5(-6+31f_S-41f_S^2+10f_S^3) - 2f_B^3(-15(9+8\lambda) + (738+924\lambda+320\lambda^2)f_S \\ & \left. - 66(9+4\lambda)f_S^2 + 297f_S^3) \right) \end{aligned} \quad (\text{B11})$$

$$\begin{aligned} \tilde{V}_{12} = & \frac{P\kappa_5 f_B f_S}{96r^4 f_B^2 \zeta_B^2} \left(3(45+44\lambda-51f_S)f_S^2 + 27f_B^5 f_S(10-41f_S+25f_S^2) + 3f_B f_S(-6(9+8\lambda) - 5(33+32\lambda)f_S + 189f_S^2) \right. \\ & + 6f_B^3(-16(9+17\lambda+8\lambda^2) + (438+856\lambda+384\lambda^2)f_S - (189+400\lambda)f_S^2 - 63f_S^3) - 9f_B^4(16(1+\lambda) - 8(23+22\lambda)f_S \\ & \left. + 3(71+52\lambda)f_S^2 - 51f_S^3) - 2f_B^2(8(1+\lambda)(9+8\lambda)^2 - 12(9+46\lambda+32\lambda^2)f_S - 3(369+308\lambda)f_S^2 + 585f_S^3) \right) \end{aligned} \quad (\text{B12})$$

$$\begin{aligned} \tilde{V}_{13} = & -\frac{(1-f_B)f_S}{32r^2 f_B^2 \zeta_B^2} \left(9(1+\lambda)f_S^2 - f_B f_S(2(9+17\lambda+8\lambda^2) + (12+13\lambda)f_S + 9f_S^2) + 3f_B^4 f_S(10-53f_S+55f_S^2) \right. \\ & + f_B^2(8(9+17\lambda+8\lambda^2) - 6(15+22\lambda+8\lambda^2)f_S + (78+63\lambda)f_S^2 + 27f_S^3) - f_B^3(-24(1+\lambda) + 2(9+13\lambda)f_S \\ & \left. + 3(4+9\lambda)f_S^2 + 87f_S^3) \right) \end{aligned} \quad (\text{B13})$$

$$\tilde{W}_{21} = 0 \quad (\text{B14})$$

$$\tilde{W}_{22} = \frac{f_S}{r} \left(f_B + f_S - 2f_B f_S \right) \quad (\text{B15})$$

$$\tilde{W}_{23} = -\frac{P\kappa_5(1+3f_B)f_S^2}{8r f_B \zeta_B} \quad (\text{B16})$$

$$\tilde{V}_{21} = -\frac{P\kappa_5 f_S}{8r^2 f_B \zeta_B} \left(9+8\lambda+3f_B(1-f_S) - 9f_S \right) \quad (\text{B17})$$

$$\tilde{V}_{22} = \frac{f_S}{8r^2} \left(16(1+\lambda) + \frac{3(1-f_B)(1-f_S)(1+3f_B)^2 f_S}{f_B \zeta_B} \right) \quad (\text{B18})$$

$$\tilde{V}_{23} = -\frac{P\kappa_5 f_S}{4r^2 f_B \zeta_B} \left(2(1+\lambda) - (1-3f_B)f_S \right) \quad (\text{B19})$$

$$\tilde{W}_{31} = 0 \quad (\text{B20})$$

$$\tilde{W}_{32} = 0 \quad (\text{B21})$$

$$\tilde{W}_{33} = -\frac{f_B f_S}{8r f_B \zeta_B} \left((21 + 16\lambda - 27f_S)f_S - 2f_B(9 + 8\lambda - 3f_S)(1 + 2f_S) + f_B^2(-6 - 39f_S + 87f_S^2) \right) \quad (\text{B22})$$

$$\tilde{V}_{31} = -\frac{3(1 - f_B)f_S}{8r^2 f_B \zeta_B} \left(f_S(-9 - 8\lambda + 3f_S) + f_B^2(6 - 9f_S + 9f_S^2) + 2f_B(9 + 8\lambda - (27 + 20\lambda)f_S + 18f_S^2) \right) \quad (\text{B23})$$

$$\begin{aligned} \tilde{V}_{32} = & \frac{P\kappa_5 f_B f_S}{4r^4 f_B \zeta_B} \left(f_S(-5(9 + 8\lambda) + 33f_S) + 9f_B^3(2 + f_S + f_S^2) - f_B(2(63 + 128\lambda + 64\lambda^2) - (99 + 112\lambda)f_S + 9f_S^2) \right. \\ & \left. + 3f_B^2(4 - 3(7 + 8\lambda)f_S + 21f_S^2) \right) \quad (\text{B24}) \end{aligned}$$

$$\begin{aligned} \tilde{V}_{33} = & \frac{f_S}{4r^2 f_B \zeta_B} \left(-3(1 + \lambda)f_S + f_B^2(-36 - 38\lambda + (57 + 39\lambda)f_S - 42f_S^2) + f_B(30 + 46\lambda + 16\lambda^2 - (33 + 28\lambda)f_S \right. \\ & \left. + 12f_S^2) + 3f_B^3(-2 - 7f_S + 14f_S^2) \right) \quad (\text{B25}) \end{aligned}$$

2. Type-II, $l = 1$

In the special case $l = 1$ the Type-II perturbation fields are $\{H_0, H_1, H_2, H_3, H_4, H_5, f_{t\theta}^-, f_{r\theta}^-, f_{\theta\phi}^-\}$, as K is not defined for $l < 2$. In addition, by applying the Fourier decomposition (A5) and assuming $\sigma = 0$, one notices that $H_4, H_5, f_{y\theta}^-$ decouple from the rest and can, thus, be neglected. Furthermore, because f_{AB} are perturbations of a Maxwell tensor derived from a vector potential, one can check that $\{f_{t\theta}^-, f_{r\theta}^-, f_{\theta\phi}^-\}$ are related via $f_{t\theta}^- = -i\omega f_{\theta\phi}^-$ and $f_{r\theta}^- = \partial_r f_{\theta\phi}^-$. After some algebraic manipulations, one can show that H_0 and H_2 can be recast as functions of the remaining perturbation fields, by using the (r, r) and (t, r) components of the perturbed Einstein equations. What remains is the group of variables $\{H_1, H_3, f_{\theta\phi}^-\}$. The first variable satisfies a first order equation in r given by the (t, ϕ) component of the Einstein equations; H_3 satisfies a second order equation constructed as an appropriate combination of the (t, t) , (y, y) and (θ, θ) components; and, finally, a second order equation for $f_{\theta\phi}^-$ is obtained from the perturbed Maxwell equations.

Now, we introduce two dynamical variables, Υ_i with $i = 1, 2$, and the constrained variable Λ that relate to $\{H_1, H_3, f_{\theta\phi}^-\}$ via

$$H_1 = \Lambda - \frac{2r}{f_S(1 + 3f_B)} H_3, \quad (\text{B26})$$

$$\begin{aligned} H_3 = & \left[\left(1 - \frac{4P^2\kappa_5^2}{(3 - f_S)(9r^2 - 2P^2\kappa_5^2 - 3r^2f_S)} \right) \frac{1}{rf_B^2} \Upsilon_1 \right. \\ & \left. + \frac{2P\kappa_5}{f_B(9r^2 - 2P^2\kappa_5^2 - 3r^2f_S)} \Upsilon_2 \right. \\ & \left. - \frac{(1 - f_B)(1 + 3f_B)f_S}{3rf_B(3 - f_S + f_B(1 - 3f_S))} \Lambda \right], \quad (\text{B27}) \end{aligned}$$

$$\begin{aligned} f_{\theta\phi}^- = & \kappa_5^{-1} \left[\Upsilon_2 - \left(\frac{2P\kappa_5}{rf_B(3 - f_S)} \right) \Upsilon_1 \right. \\ & \left. + \frac{P\kappa_5 f_S(1 + 3f_B)}{3r(3 - f_S + f_B(1 - 3f_S))} \Lambda \right]. \quad (\text{B28}) \end{aligned}$$

The introduction of the auxiliary variables $\{\Lambda, \Upsilon_1, \Upsilon_2\}$ allows us to recast the second order equations for $\{H_3, f_{\theta\phi}^-\}$ (which featured source terms proportional to $\{H_1, H_3, f_{\theta\phi}^-\}$ and derivatives thereof) into a pair of coupled second-order equations that only contain $\{\Upsilon_i, \partial_r \Upsilon_i, \partial_r^2 \Upsilon_i\}$, which we listed in Eqs. (5). Finally, the ansatz (B26) allows us to realize that Λ is related to the remaining two variables via a differential constrained equation that closes the system:

$$\partial_r \Lambda + \mu_0 \Lambda + \mu_1 \Upsilon_1 + \mu_2 \Upsilon_2 = 0 \quad (\text{B29})$$

where

$$\mu_0 = \left(\frac{1}{rf_B f_S (1+3f_B)(-3+f_S+f_B(-1+3f_S))} \cdot \left(-3+3f_B^3(-1+f_S)+4f_S-f_S^2+f_B^2(-13+30f_S-9f_S^2)+f_B(-13+11f_S-6f_S^2) \right) \right), \quad (\text{B30})$$

$$\mu_1 = \frac{1}{r^3 f_B f_S^2} \left(\frac{4P^2 \kappa_5^2 f_S}{3-f_S} - \frac{3r^2(3+f_B)(1-f_S)}{(1+3f_B)^2} \cdot \left(1 + \frac{2}{3-f_S} - \frac{6r^2}{9r^2-2P^2\kappa_5^2-3r^2f_S} \right) \right), \quad (\text{B31})$$

$$\mu_2 = -\frac{2P\kappa_5}{f_S^2} \left(\frac{f_S}{r^2} + \frac{3(3+f_B)(1-f_S)}{(1+3f_B)^2(9r^2-2P^2\kappa_5^2-3r^2f_S)} \right). \quad (\text{B32})$$

For completeness, here we list the full expressions of the coefficients in Eqs. (5):

$$W_{11} = \frac{f_S}{r(1+3f_B)(3-f_S)(2+f_B(1-f_S))^2} \cdot \left(-12(-3+f_S)f_S+3f_B^4(-1+f_S)^2(3+f_S+2f_S^2)+4f_B(3+14f_S-21f_S^2+4f_S^3)+f_B^2(48-119f_S+23f_S^2+27f_S^3-3f_S^4)+f_B^3(39-174f_S+208f_S^2-74f_S^3+f_S^4) \right) \quad (\text{B33})$$

$$V_{11} = \frac{f_S}{r^2(1+3f_B)^2(3-f_S)^2(2+f_B(1-f_S))^3(3-f_S+f_B(1-3f_S))^2} \cdot \left(12(-3+f_S)^3 f_S(-21+f_S^2)+54f_B^9(-1+f_S)^4(-3-2f_S+f_S^2)-4f_B(-3+f_S)^2(-63-876f_S+1315f_S^2-273f_S^3+f_S^5)+9f_B^8(-1+f_S)^3(87+96f_S+124f_S^2-250f_S^3-27f_S^4+18f_S^5)+3f_B^7(-1+f_S)^2(921-5782f_S+7581f_S^2-7268f_S^3+6123f_S^4-1446f_S^5+63f_S^6)+f_B^6(60060-306980f_S+685662f_S^2-771836f_S^3+423070f_S^4-95500f_S^5+3178f_S^6+1260f_S^7-66f_S^8)+f_B^5(25230-141257f_S+348325f_S^2-501473f_S^3+427073f_S^4-194707f_S^5+39335f_S^6-2499f_S^7-27f_S^8)+f_B^4(59529-283361f_S+456189f_S^2-253885f_S^3-15645f_S^4+54653f_S^5-15265f_S^6+1249f_S^7-8f_S^8)+f_B^3(11016+40185f_S-177621f_S^2+197161f_S^3-87965f_S^4+17235f_S^5-1303f_S^6+11f_S^7+f_S^8)+f_B^2(26703-71064f_S-52318f_S^2+230692f_S^3-189036f_S^4+61632f_S^5-8202f_S^6+308f_S^7+5f_S^8) \right) \quad (\text{B34})$$

$$W_{12} = -\frac{4P\kappa_5 f_S^2}{3r^2(1+3f_B)(2+f_B(1-f_S))^2} (9-f_S+5f_B(1-f_S)-6f_B^2(1-f_S)) \quad (\text{B35})$$

$$V_{12} = \frac{-2P\kappa_5 f_S}{3r^3(1+3f_B)^2(2+f_B(1-f_S))^3(3-f_S+f_B(1-3f_S))^2} \cdot \left(27f_B^7(-1+f_S)^3(1+f_S)-2(-3+f_S)^2(-54+180f_S-23f_S^2+f_S^3)+9f_B^6(-1+f_S)^2(-19-15f_S-21f_S^2+15f_S^3)+f_B^5(9709-29512f_S+37424f_S^2-23938f_S^3+6915f_S^4-598f_S^5)+f_B^4(11733-33209f_S+38666f_S^2-19922f_S^3+3857f_S^4-229f_S^5)+f_B(5868-17997f_S+18076f_S^2-6238f_S^3+840f_S^4-37f_S^5)+3f_B^5(38-587f_S+700f_S^2+146f_S^3-306f_S^4+9f_S^5)-2f_B^4(-1645+6227f_S-7659f_S^2+4957f_S^3-1880f_S^4+288f_S^5) \right) \quad (\text{B36})$$

$$W_{22} = \frac{f_S}{r(3-f_S)(1+3f_B)(2+f_B(1-f_S))^2} \cdot \left(-4(-3+f_S)f_S + 3f_B^4(-1+f_S)^2(3-15f_S+2f_S^2) + 4f_B(3-4f_S+5f_S^2) + f_B^3(39-80f_S+18f_S^2+24f_S^3-f_S^4) - f_B^2(-48+69f_S-5f_S^2+7f_S^3+f_S^4) \right) \quad (\text{B37})$$

$$V_{22} = \frac{f_S}{r^2(1+3f_B)^2(3-f_S)(2+f_B(1-f_S))^3(3-f_S+f_B(1-3f_S))^2} \cdot \left(54f_B^9(-1+f_S)^4(1+f_S) + 4(-3+f_S)^3(-12+7f_S+f_S^2) - 9f_B^8(-1+f_S)^3(41+9f_S+117f_S^2-105f_S^3+18f_S^4) - 4f_B(-2457+5616f_S-4716f_S^2+1666f_S^3-251f_S^4+14f_S^5) - 3f_B^7(-1+f_S)^2(1-339f_S-1954f_S^2+2718f_S^3-615f_S^4+45f_S^5) + f_B^2(25236-67251f_S+71006f_S^2-37009f_S^3+8512f_S^4-765f_S^5+14f_S^6+f_S^7) + f_B^3(22989-77809f_S+94013f_S^2-58169f_S^3+19751f_S^4-2275f_S^5-49f_S^6+13f_S^7) + f_B^4(-1195-15084f_S+29469f_S^2-13224f_S^3+1015f_S^4+724f_S^5-617f_S^6+64f_S^7) + 2f_B^5(-5978+14642f_S-14269f_S^2+13497f_S^3-11896f_S^4+4688f_S^5-753f_S^6+69f_S^7) + f_B^6(-5146+17301f_S-12032f_S^2-5489f_S^3+4038f_S^4+2123f_S^5-876f_S^6+81f_S^7) \right) \quad (\text{B38})$$

$$W_{21} = -\frac{4P\kappa_5 f_B^2 f_S^2}{r^2(1+3f_B)(3-f_S)^2(2+f_B(1-f_S))^2} \cdot \left(10+3f_B^3(-9+f_S)(-1+f_S)^2+8f_S-2f_S^2+4f_B(-6-7f_S+f_S^2)+f_B^2(-31+11f_S+23f_S^2-3f_S^3) \right) \quad (\text{B39})$$

$$V_{21} = -\frac{2P\kappa_5 f_B f_S}{r^3(1+3f_B)^2(2+f_B(1-f_S))^3(3-f_S)^3(3-f_S+f_B(1-3f_S))^2} \cdot \left(16(-3+f_S)^3 f_S(-5-4f_S+f_S^2) + 54f_B^9(-1+f_S)^4(-3-2f_S+f_S^2) - 4f_B(-3+f_S)^2(60-11f_S+187f_S^2+117f_S^3-43f_S^4+2f_S^5) - 9f_B^8(-1+f_S)^3(-129+142f_S-976f_S^2+1430f_S^3-423f_S^4+36f_S^5) + 3f_B^7(-1+f_S)^2(-189+2248f_S-18617f_S^2+25716f_S^3-7091f_S^4+420f_S^5+9f_S^6) + 2f_B^2(-4968+174f_S+7727f_S^2-1370f_S^3+1843f_S^4-2014f_S^5+581f_S^6-54f_S^7+f_S^8) + 4f_B^3(-867-5167f_S+31793f_S^2-33910f_S^3+14014f_S^4-3911f_S^5+1005f_S^6-148f_S^7+7f_S^8) + f_B^4(32142-102941f_S+246597f_S^2-377773f_S^3+249201f_S^4-79311f_S^5+14551f_S^6-1767f_S^7+101f_S^8) + f_B^5(38937-106226f_S+152024f_S^2-270874f_S^3+320770f_S^4-158742f_S^5+35856f_S^6-3870f_S^7+189f_S^8) + f_B^6(13767-29608f_S-53102f_S^2+142280f_S^3-45248f_S^4-53128f_S^5+29758f_S^6-5016f_S^7+297f_S^8) \right) \quad (\text{B40})$$

-
- [1] J. D. Bekenstein, Phys. Rev. D **7**, 2333 (1973).
[2] S. D. Mathur, Class. Quant. Grav. **26**, 224001 (2009), arXiv:0909.1038 [hep-th].
[3] I. Bena, E. J. Martinec, S. D. Mathur, and N. P. Warner, (2022), arXiv:2204.13113 [hep-th].
[4] I. Bena, E. J. Martinec, S. D. Mathur, and N. P. Warner, (2022), arXiv:2203.04981 [hep-th].
[5] I. Bena, C.-W. Wang, and N. P. Warner, JHEP **11**, 042 (2006), arXiv:hep-th/0608217.
[6] I. Bena, S. Giusto, E. J. Martinec, R. Russo, M. Shigemori, D. Turton, and N. P. Warner, Phys. Rev. Lett. **117**, 201601 (2016), arXiv:1607.03908 [hep-th].
[7] I. Bena, S. Giusto, E. J. Martinec, R. Russo, M. Shigemori, D. Turton, and N. P. Warner, JHEP **02**, 014 (2018), arXiv:1711.10474 [hep-th].
[8] I. Bah and P. Heidmann, JHEP **09**, 128 (2021), arXiv:2106.05118 [hep-th].
[9] I. Bah, P. Heidmann, and P. Weck, JHEP **08**, 269 (2022), arXiv:2203.12625 [hep-th].
[10] S. W. Hawking, Phys. Rev. D **14**, 2460 (1976).
[11] J. Polchinski, in *Theoretical Advanced Study Institute in Elementary Particle Physics: New Frontiers in Fields and Strings* (2017) pp. 353–397, arXiv:1609.04036 [hep-th].
[12] V. Balasubramanian, E. G. Gimon, and T. S. Levi, JHEP **01**, 056 (2008), arXiv:hep-th/0606118.
[13] I. Bena, N. Čeplak, S. D. Hampton, A. Houppé, D. Touloukas, and N. P. Warner, (2022), arXiv:2212.06158 [hep-th].
[14] T. Ikeda, M. Bianchi, D. Consoli, A. Grillo, J. F. Morales, P. Pani, and G. Raposo, Phys. Rev. D **104**, 066021 (2021), arXiv:2103.10960 [gr-qc].
[15] I. Bah and P. Heidmann, Phys. Rev. Lett. **126**, 151101 (2021), arXiv:2011.08851 [hep-th].

- [16] V. Cardoso and P. Pani, *Living Rev. Rel.* **22**, 4 (2019), arXiv:1904.05363 [gr-qc].
- [17] P. Heidmann, I. Bah, and E. Berti, *Phys. Rev. D* **107**, 084042 (2023), arXiv:2212.06837 [gr-qc].
- [18] P. Heidmann, N. Speeney, E. Berti, and I. Bah, *Phys. Rev. D* **108**, 024021 (2023), arXiv:2305.14412 [gr-qc].
- [19] M. Bianchi, G. Di Russo, A. Grillo, J. F. Morales, and G. Sudano, *JHEP* **12**, 121 (2023), arXiv:2305.15105 [gr-qc].
- [20] A. Dima, M. Melis, and P. Pani, (2024), arXiv:2406.19327 [gr-qc].
- [21] I. Bena, G. Di Russo, J. F. Morales, and A. Ruipérez, (2024), arXiv:2406.19330 [hep-th].
- [22] M. Bianchi, D. Bini, and G. Di Russo, (2024), arXiv:2407.10868 [gr-qc].
- [23] M. Bianchi, D. Bini, and G. Di Russo, (2024), arXiv:2411.19612 [gr-qc].
- [24] R. Gregory and R. Laflamme, *Phys. Rev. Lett.* **70**, 2837 (1993), arXiv:hep-th/9301052.
- [25] U. Miyamoto and H. Kudoh, *JHEP* **12**, 048 (2006), arXiv:gr-qc/0609046.
- [26] S. Stotyn and R. B. Mann, *Phys. Lett. B* **705**, 269 (2011), arXiv:1105.1854 [hep-th].
- [27] I. Bah, A. Dey, and P. Heidmann, *JHEP* **04**, 168 (2022), arXiv:2112.11474 [hep-th].
- [28] V. Cardoso, S. Hopper, C. F. B. Macedo, C. Palenzuela, and P. Pani, *Phys. Rev. D* **94**, 084031 (2016), arXiv:1608.08637 [gr-qc].
- [29] V. Cardoso, E. Franzin, and P. Pani, *Phys. Rev. Lett.* **116**, 171101 (2016), [Erratum: *Phys. Rev. Lett.* **117**, 089902 (2016)], arXiv:1602.07309 [gr-qc].
- [30] V. Cardoso and P. Pani, *Nature Astron.* **1**, 586 (2017), arXiv:1709.01525 [gr-qc].
- [31] I. Bah and P. Heidmann, *JHEP* **09**, 147 (2021), arXiv:2012.13407 [hep-th].
- [32] Y.-K. Lim, *Phys. Rev. D* **103**, 084044 (2021), arXiv:2102.08531 [gr-qc].
- [33] V. Cardoso, L. C. B. Crispino, C. F. B. Macedo, H. Okawa, and P. Pani, *Phys. Rev. D* **90**, 044069 (2014), arXiv:1406.5510 [gr-qc].
- [34] W.-D. Guo, Q. Tan, and Y.-X. Liu, *Phys. Rev. D* **107**, 124046 (2023), arXiv:2212.08784 [gr-qc].
- [35] W.-D. Guo and Q. Tan, *Universe* **9**, 320 (2023), arXiv:2402.14265 [gr-qc].
- [36] D. Pereñíguez, *Phys. Rev. D* **108**, 084046 (2023), arXiv:2302.10942 [gr-qc].
- [37] P. Pani, *Int. J. Mod. Phys. A* **28**, 1340018 (2013), arXiv:1305.6759 [gr-qc].
- [38] P. Pani, V. Cardoso, L. Gualtieri, E. Berti, and A. Ishibashi, *Phys. Rev. D* **86**, 104017 (2012), arXiv:1209.0773 [gr-qc].
- [39] R. H. Price, *Phys. Rev. D* **5**, 2439 (1972).
- [40] P. V. P. Cunha, E. Berti, and C. A. R. Herdeiro, *Phys. Rev. Lett.* **119**, 251102 (2017), arXiv:1708.04211 [gr-qc].
- [41] F. C. Eperon, H. S. Reall, and J. E. Santos, *JHEP* **10**, 031 (2016), arXiv:1607.06828 [hep-th].
- [42] J. Keir, *Class. Quant. Grav.* **33**, 135009 (2016), arXiv:1404.7036 [gr-qc].